Electronic supplementary materials *Mendeleev Commun.*, 2025, **35**, 228–230

Selective hydrogenation of nitrobenzene to aniline over $LaNiO_3$

Olga P. Tkachenko, Elena V. Shuvalova, Petr V. Zemlianskii, Nikolay A. Davshan and Leonid M. Kustov

Hydrogenation experiments.

Catalyst preparation & characterization

For the $LaNiO_3$ synthesis, $La(NO_3)_3 \cdot 6H_2O$ and $Ni(NO_3)_2 \cdot 6H_2O$ were dissolved in distilled water in the equimolar ratio. The Ni concentration was 0.2 M. The prepared water solution of glycine was added dropwise to the nitrate solution. The glycine/(La^{3+} + Ni^{2+}) molar ratio was 5:1. The mixture was stirred for 24 h, then dried at 120°C for 5 h and calcined at 600°C for 5 h. The final products were marked as $LaNiO_3$-glyc.

Specific surface area measurements were carried out by the nitrogen adsorption-desorption method using an ASAP 2020 Plus unit (Micromeritics) at 77 K according to ISO 9277-2010. The BET surface area of $LaNiO_3$-glyc. was 10.1 m^2/g.

The X-ray powder diffraction measurements were performed using an Empyrean (PANalytical) diffractometer equipped with a linear position-sensitive X'Celerator detector. Ni-filtered CuK_α radiation was employed. Standard Bragg-Brentano (reflection) geometry was used. The powder of $LaNiO_3$ was carefully fixed onto a silicon zero background holder and X-ray patterns from 10° to 80° 2θ were recorded at room temperature.

The EM observations were carried out using a Hitachi Regulus8230 field-emission scanning electron microscope (FE-SEM). Images were acquired in secondary electrons at a 5 kV accelerating voltage. EDS-SEM studies were carried out using a Bruker Quantax 400 EDS system equipped with an XFlash 6|60 detector at a 20 kV accelerating voltage. A target-oriented approach was utilized for the optimization of the analytic measurements.[S1] (Before measurements, the sample was mounted on a 25 mm aluminum specimen stub, fixed by a conductive carbon tape and coated with a 10 nm film of carbon. The observations were carried out using a Hitachi Regulus8230 field-emission scanning electron microscope (FE-SEM). Images were acquired in secondary electrons at a 5 kV accelerating voltage. EDS-SEM studies were carried out using a Bruker Quantax 400 EDS system equipped with an XFlash 6|60 detector at a 20 kV accelerating voltage.

Hydrogenation experiments.

The batch mode tests were performed in a Teflon-lined 100 mL autoclave at 150 °C and the initial H_2 pressure 1.5 MPa The specified amounts of substrate 220 mg and solvent ethanol 20 cm^3 were introduced into the reactor, and the mixtures were vigorously stirred for 5 min to form solutions with a substrate, then 0.100 g of internal standard $C_{10}H_{22}$ was added into the solution. Before catalyst addition the stirring was stopped, and the probe of the initial solution was taken for analysis. Then the reactor was closed and preliminarily flushed with hydrogen three times up to 0.5 MPa, and finally the pressure was adjusted to 1.5 MPa at room temperature. The reaction was started by stirring after heating to the required temperature.

The time dependence curves of a substrate conversion and selectivity to the aniline were constructed analyzing the liquid probes withdrawn from the reactor every 1 hour using a special high-pressure sampling valve. The CrystaLux 4000M GC instrument equipped with a 30 m × 0.25 mm capillary S2 column Optima-1 (Macherey-Nagel) was used to carry out a probe analysis: the column was heated to 140 °C. The analyst to standard peak area ratio was used to determine the concentrations of substrates and aniline detected by GC in the reaction mixture. The substrate conversion and the selectivity to aniline were calculated based on the changes in the relative concentrations, which were corrected as to the area of a standard peak in an initial reaction mixture. We did not make any attempt to reveal and identify intermediate hydroxyamino, azoxy, hydrazo and azo products because they were not of interest for our investigation.

XPS study

X-ray photoelectron spectra were recorded using a modernized ES-2403 spectrometer equipped with a PHOIBOS 100-5MCD energy analyzer and an XR-50 X-ray source (Specs GmbH, Germany). The spectrometer was preliminarily calibrated according to the binding energy of the Au $4f_{7/2}$ level (84.0 eV) and Ni $2p_{3/2}$ (852.7 eV). For photoelectron excitation, characteristic radiation of Al Kα (1486.6 eV) and Mg Kα (1253.6 eV) with a power of 250 W was used.

Survey spectra were recorded with a step of 0.5 eV and a dwell time of 0.4 sec at a point. XPS spectra of C 1s, O 1s, La 3d, and Ni 2p electrons were recorded with a step of 0.1 eV. The line of C 1s electrons with the binding energy E_b = 285.0 eV (typical alkane surface contaminants) was used as an external standard. High-resolution spectra were recorded in steps of 0.1 eV. Spectra were obtained using a standard SpecsLab2 software. The CasaXPS software package was used to analyze the spectra.

The atomic ratio of elements (with an accuracy of ± 10% rel.) in the surface layers accessible to XPS analysis (20-30 Å) was calculated from the integral line intensity corrected for

the Scofield photoionization cross section,[S2] the depth of free photoelectron leakage and the energy dependence of the transmittance analyzer. Model decomposition of high-resolution spectra in order to isolate individual states was carried out taking into account such characteristics of photoelectron sublevels as the binding energy of the components, the ratio of the areas of the components, and spin-orbit splitting.

Powdered catalyst samples were fixed in a holder using a special conductive double-sided adhesive tape and were preliminarily degassed. The spectra were recorded in a vacuum of no worse than 1 x 10^{-9} Torr. For photoelectron excitation, characteristic radiation of Al Kα (1486.6 eV) and Mg Kα (1253.6 eV) with a power of 250 W was used. Survey spectra were recorded with a step of 0.5 eV and a dwell time of 0.4 sec at a point. XPS spectra of C 1s, O 1s, La 3d, and Ni 2p electrons were recorded with a step of 0.1 eV.

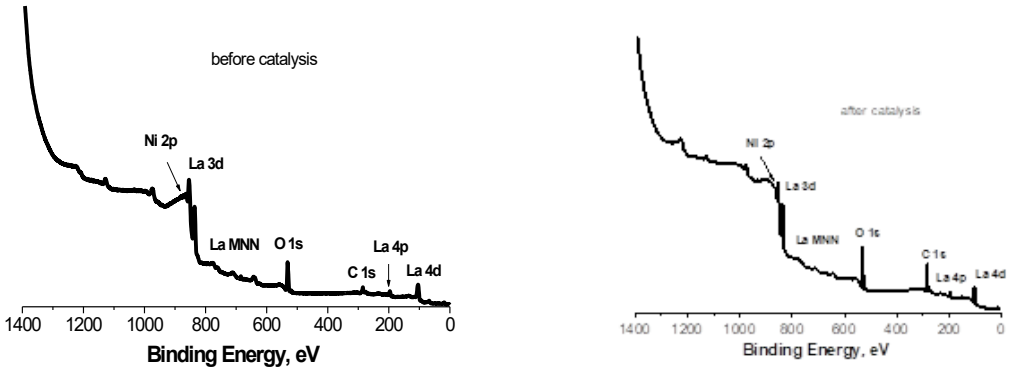

Figure S1. Survey XP spectrum of $LaNiO_3$-glyc (before and after catalysis).

It can be seen that the survey spectra of the studied samples are of the same type. The surface typically contains carbon and oxygen, as well as lanthanum and nickel. In both figures, photoelectron lines of carbon C 1s and oxygen O 1s are visible. In addition, photoelectron lines of La 4d, La 4p, La 3d and weak Auger electron lines of La MNN are clearly visible.

Figures S2-S5 present high-resolution photoelectron spectra of La 3d, and Ni 2p.

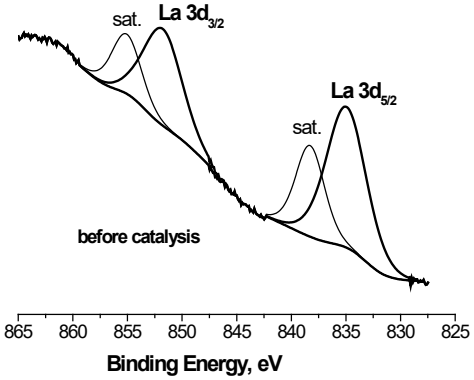

Figure S2. XP La 3d spectra before catalysis.

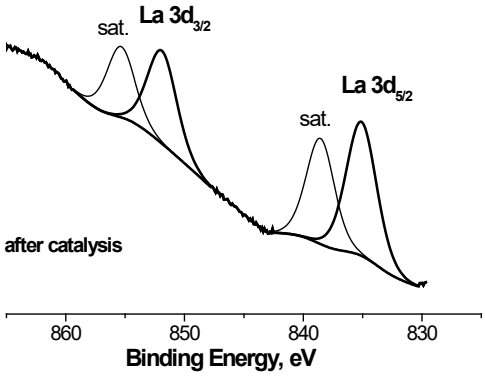

Figure S3. XP La 3d spectra after catalysis.

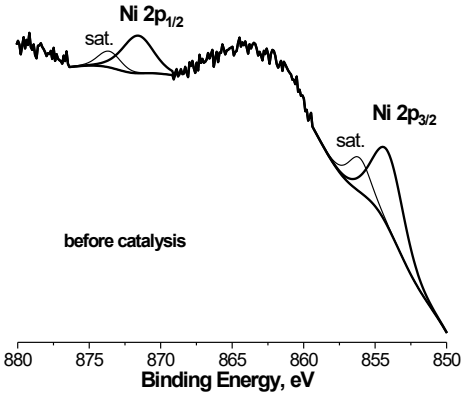

Figure S4. XP Ni 2p spectra before catalysis.

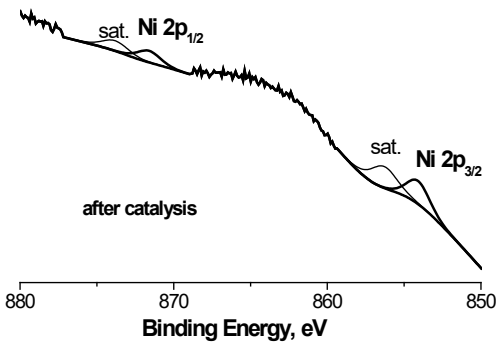

Figure S5. XP Ni 2p spectra before catalysis.

Figures S6 and S7 depict SEM micrographs of the $LaNiO_3$-glyc sample before and after catalysis, respectively.

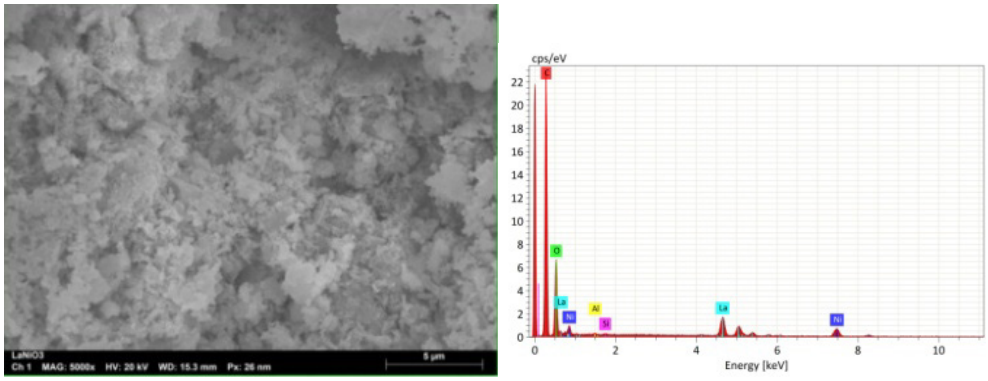

Figure S6 SEM image and EDS analysis of the fresh catalyst.

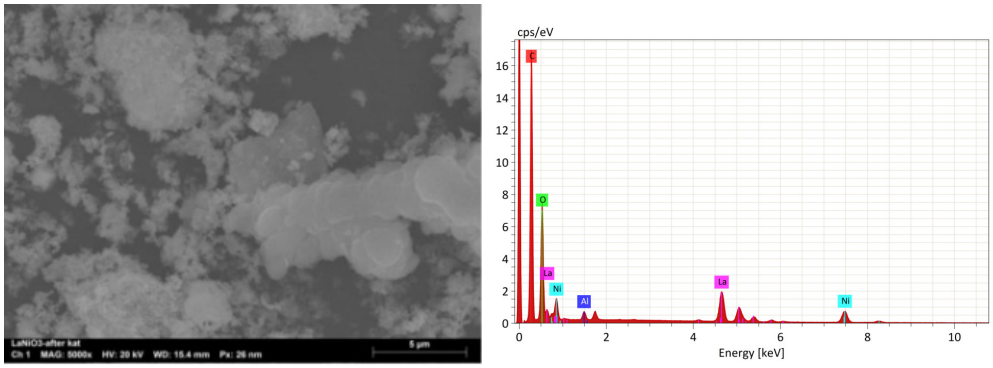

Figure S7 SEM image and EDS analysis of the spent catalyst.

The SEM images clearly show the enlargement of $LaNiO_3$-glyc perovskite particles during the catalysis process compared to the sample before catalysis.

Table S1 EDS data for $LaNiO_3$-glyc.

Element	Before catalysis		After catalysis	
	Mass %	Atom %	Mass %	Atom %
Oxygen	49.50	28.39	52.02	32.76
Carbon	91.08	69.58	76.80	64.43
Lanthanum	14.91	**0.99**	17.47	**1.27**
Nickel	6.16	**0.96**	7.23	**1.24**
Aluminum	0.17	0.06	0.82	0.30
Silicon	0.10	0.03	-	-

The EDS data (Table S1) showed a slight difference in the percentages of lanthanum and nickel in the samples before and after catalysis. The La/Ni atomic ratio in both samples is the same and close to 1. The significant difference in the atomic ratio obtained from XPS data (see Table 1 of the main text) and EDS can be explained by a significant difference in the depth of the analyzed layer (20-30 A in XPS *vs* 1 μm in EDS).

To confirm the crystal structure of $LaNiO_3$-glyc., XRD study was used (Figure. 6). The X-ray diffraction profile of $LaNiO_3$-glyc. shows four main reflections at 2θ = 33.02°; 47.47°; 57.87° and 58.88° and six low-intensity reflections at 40.98°; 53.83°; 68.93°; 69.85°; 78.62° and 79.53°, which correspond to the characteristic diffraction lines of crystalline $LaNiO_3$, in agreement with the JCPDS card no. 00-034-1181. In addition, there are four reflections at 37.49°; 43.54°; 63.09° and 75.60°, which correspond to the characteristic diffraction lines of crystalline NiO, in agreement with the JCPDS card no 01-078-0643. Four small reflections belonging to crystalline $La_2O_2CO_3$ at 24.24°; 29.28°; 30.18° and 31.55° in agreement with the JCPDS card no 00-048-1113 and four small reflections belonging to $La(OH)_3$ hydroxide at 15.94°; 27.53°; 28.18° and 39.78° in agreement with the JCPDS card no 00-036-1481 were observed.

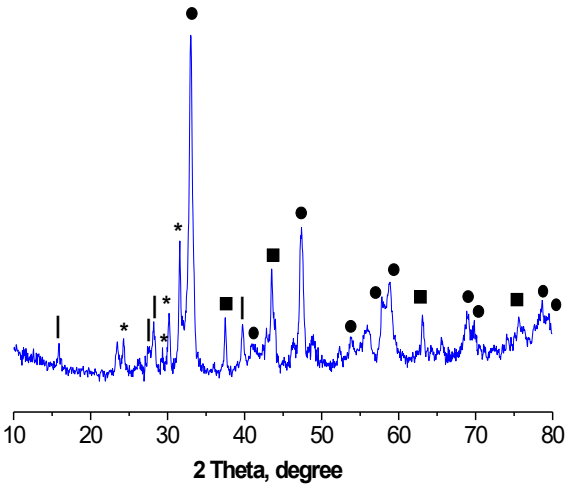

Figure S8 Powder XRD pattern of $LaNiO_3$ perovskite.

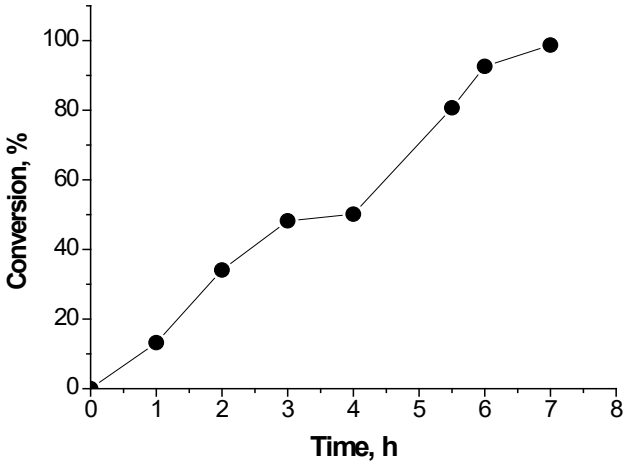

Figure S9 Dependence of the total conversion of nitrobenzene on the reaction time.

Table S2 Comparison of the efficiency of Ni-containing catalysts in the hydrogenation of nitrobenzene into aniline

Catalyst	Reaction condition	$PhNO_2$ conversion, %	Selectivity to $PhNH_2$ %	Reference
20%Ni/Bentonite	Gas phase, 300 °C, 10 h	95.7	98.8	S3
36%Ni/ γ-Al_2O_3	35-50 °C, EtOH, 2-6 MPa H_2, 50 min	13	89	S4
88.2 m^2/g 4.6%/KIT-6	90 °C, EtOH, 1 MP H_2, 1 h	100	100	S5
10%Ni/C mineral	90 °C, EtOH, 2 MPa H_2, 1 h	1.2-64.9	100	S6
2.8%Ni/ SiO_2	40 °C, 10 bar H_2, EtOH, 16 h	100	80	S7
79.6% Ni/C	120 °C, EtOH, 1.5 MPa H_2, 2 h	67	99	S8
$LaNiO_3$ (10% Ni)	150 °C EtOH, 1.5 MPa H_2, 7 h	98.7	95.6	This work

References

S1. V. V. Kachala, L. L. Khemchyan, A. S. Kashin, N. V. Orlov, A. A. Grachev, S. S. Zalesskiy and V. P. Ananikov, *Russ. Chem. Rev.*, 2013, **82**, 648; https://doi.org/10.1070/RC2013v082n07ABEH004413.

S2. J. H. Scofield, *J. Electron Spectrosc.*, 1976, **8**, 129; https://doi.org/10.1016/0368-2048(76)80015-1.

S3. Y. Jiang, X. Li, Z. Qin and H. Ji, *Chin. J. Chem. Eng.*, 2016, **24**, 1195; https://doi.org/10.1016/j.cjche.2016.04.030.

S4. X. Meng, H. Cheng, Y. Akiyama, Y. Hao, W. Qiao, Y. Yu, F. Zhao, S.-I. Fujita and M. Arai, *J. Catal.*, 2009, **264**, 1; https://doi.org/10.1016/j.jcat.2009.03.008.

S5. X. Zhou, H. Zhao, S. Liu, D. Ye, R. Qu, C. Zheng and X. Gao, *Appl. Surf. Sci.*, 2020, **525**, 146382; https://doi.org/10.1016/j.apsusc.2020.146382.

S6. E. N. Terekhova, O. B. Belskaya, R. R. Izmaylov, M. V. Trenikhin and V. A. Likholobov, *Catalysts,* 2023, **13**(1), 82; https://doi.org/10.3390/catal13010082.

S7. B. Klausfelder and R. Kempe, *Z. Anorg. Allg. Chem.,* 2023, **649**, e202300071; https://doi.org/10.1002/zaac.202300071.

S8. A. Das, K. M. Hansda, A. Mahato, P. Singh and N. Mahata, *J. Indian Chem. Soc.*, 2020, **97**, 2948; https://doi.org/10.5281/zenodo.5654751.